



**HAL**  
open science

## **N<sub>2</sub><sup>+</sup> fluorescence spectrum of comet C/2016 R2 (PanSTARRS)**

P. Rousselot, S. E. Anderson, A. Alijah, B. Noyelles, C. Opitom, E. Jehin, D.  
Hutsemékers, J. Manfroid

► **To cite this version:**

P. Rousselot, S. E. Anderson, A. Alijah, B. Noyelles, C. Opitom, et al.. N<sub>2</sub><sup>+</sup> fluorescence spectrum of comet C/2016 R2 (PanSTARRS). *Astronomy and Astrophysics - A&A*, 2022, 661, pp.A131. 10.1051/0004-6361/202142829 . hal-03679664

**HAL Id: hal-03679664**







**<https://hal.science/hal-03679664v1>**

Submitted on 26 May 2022

**HAL** is a multi-disciplinary open access archive for the deposit and dissemination of scientific research documents, whether they are published or not. The documents may come from teaching and research institutions in France or abroad, or from public or private research centers.

L'archive ouverte pluridisciplinaire **HAL**, est destinée au dépôt et à la diffusion de documents scientifiques de niveau recherche, publiés ou non, émanant des établissements d'enseignement et de recherche français ou étrangers, des laboratoires publics ou privés.

# $N_2^+$ fluorescence spectrum of comet C/2016 R2 (PanSTARRS)

P. Rousselot<sup>1</sup> , S. E. Anderson<sup>1</sup>, A. Alijah<sup>2</sup> , B. Noyelles<sup>1</sup> , C. Opitom<sup>3</sup> , E. Jehin<sup>4</sup> ,  
D. Hutsemékers<sup>4</sup>, and J. Manfroid<sup>4</sup> 

<sup>1</sup> Institut UTINAM, UMR 6213 CNRS–Univ. Bourgogne Franche-Comté, OSU THETA, BP 1615, 25010 Besançon Cedex, France  
e-mail: [philippe.rousselot@obs-besancon.fr](mailto:philippe.rousselot@obs-besancon.fr)

<sup>2</sup> GSMA, UMR CNRS 7331, UFR Sciences Exactes et Naturelles, Univ. of Reims Champagne-Ardenne, 51100 Reims, France

<sup>3</sup> Institute for Astronomy, Univ. of Edinburgh, Royal Observatory, Edinburgh EH9 3HJ, UK

<sup>4</sup> STAR Institute, Univ. of Liège, Allée du 6 Août 19c, 4000 Liège, Belgium

Received 3 December 2021 / Accepted 14 February 2022

## ABSTRACT

**Context.**  $N_2$  is rarely found in comets, or when it is present, it is found only in small quantities despite its abundance on the surfaces of different outer Solar System objects. A few comets presented  $N_2^+$  emission lines in their optical spectra. One of them, C/2016 R2, showed an unusually high abundance of this species in 2018, with dozens of bright  $N_2^+$  emission lines. A robust model of the  $N_2^+$  fluorescence in comets would permit us to perform a detailed quantitative analysis of this species and enlarge our comprehension of the surprisingly wide range of  $N_2$  abundances in comets.

**Aims.** The goal of this work is to provide the necessary tools to interpret  $N_2^+$  spectra. Computing production rates for a cometary species necessitates a good knowledge of the number of molecules located along the line of sight of the spectrometer. This in turn requires a good modeling of the emission spectrum with detailed fluorescence efficiencies for the different bands.

**Methods.** We developed a model based on available laboratory data and new theoretical results relative to the  $N_2^+$  to compute the emission spectrum of this species observed in 8.2 m Very Large Telescope high-resolution spectra of comet C/2016 R2. Because of some significant differences between spectra obtained on the nucleus and at a cometocentric distance of about 6000 km, it became apparent that a classic fluorescence equilibrium spectrum could not be used. A synthetic spectrum based on a Monte Carlo method and producing spectra at different times from an initial relative population was developed and compared to our observational data.

**Results.** Our modeling of the cometary  $N_2^+$  emission spectrum satisfactorily fits our observed spectra of comet C/2016 R2, leading to the first modeling at high resolution. Different fluorescence efficiency factors are computed.

**Key words.** comets: general – comets: individual: C/2016 R2 – molecular data

## 1. Introduction

Comets are small icy bodies that have undergone little alteration since their formation in the outer part of the Solar System. Studying their composition provides insight into the primitive Solar System and into the physical and chemical properties of their formation place. Many studies have shown that comets present a variety of compositions. A typical cometary coma contains mostly water molecules with CO and CO<sub>2</sub> as the second species (typically about 10–20% relative to water). The relative abundances of the other species can vary significantly among comets, such as C<sub>2</sub> and C<sub>3</sub> in carbon-chain-depleted comets.

Nitrogen atoms are usually found in molecules such as NH<sub>3</sub> or HCN (their dissociation products NH<sub>2</sub> and CN have bright emission lines at optical wavelengths). Surprisingly, N<sub>2</sub> is usually not detected in cometary comae, even though both Pluto and Triton, which also formed in the outer Solar System, exhibit an N<sub>2</sub>-rich surface (Cruikshank et al. 1993; Owen et al. 1993; Quirico et al. 1999; Merlin et al. 2018). No emission lines of the N<sub>2</sub> molecule itself appear in the visible range, but this molecule can be ionized to N<sub>2</sub><sup>+</sup>. The emission lines of this ion are clearly detectable in the optical range. The brightest band is the (0, 0) with a bandhead near 3914 Å. Until recently, only a few detections of N<sub>2</sub><sup>+</sup> emission lines in comets have been reported from ground-based facilities. This mainly concerns the following comets: C/1908 R1 (Morehouse; de La Baume Pluvinel & Baldet 1911), C/1961 R1 (Humason; Greenstein 1962), 1P/Halley

(Wyckoff & Theobald 1989; Lutz et al. 1993), C/1987 P1 (Bradfield; Lutz et al. 1993), 29P/Schwassmann-Wachmann 1 (Korsun et al. 2008; Ivanova et al. 2016, 2018), and C/2002 VQ94 (LINEAR; Korsun et al. 2008, 2014). It should be noted that some spectra might have been contaminated by telluric N<sub>2</sub><sup>+</sup> emission lines. The first in situ detection of N<sub>2</sub> in a comet was reported in the coma of 67P by the ROSINA mass spectrometer on board the Rosetta spacecraft (Rubin et al. 2015); the N<sub>2</sub>/H<sub>2</sub>O ratio was  $8.9 \times 10^{-4}$  near perihelion (Rubin et al. 2020).

The interpretation of this N<sub>2</sub> depletion in comets is a matter of debate in the scientific community and could provide interesting constraints on the formation process of comets. It was interpreted as the result of the selective trapping of CO at the expense of N<sub>2</sub> in the building blocks of comets presumably agglomerated from clathrates (Iro et al. 2003), or as the result of their partial devolatilization due to radiogenic heating (Mousis et al. 2012). One scenario for the only comet rich in N<sub>2</sub> observed in the recent years with a large telescope (see below) is that it formed in a colder environment than the other comets, which share more typical compositions (Mousis et al. 2021). In any case, constraining the N<sub>2</sub> abundance in comets provides important constraints on the formation scenario of comets.

In this context, a surprising comet, detected on September 7, 2016, by the Panoramic Survey Telescope And Rapid Response System (PanSTARRS; Weryk & Wainscoat 2016) presented an unusual composition during its perihelion passage at the end of 2017 and the beginning of 2018 at a distance of 2.8 au. Called

C/2016 R2 (PanSTARRS), it is a returning comet (i.e., a nearly isotropic comet with a semimajor axis smaller than 10 000 au (see [Levison 1996](#)). It comes from the Oort cloud, and has a period of about 20 000 yr and a semimajor axis of 735 au. Nicknamed “the blue comet”, it developed a coma at large ( $\sim 6$  au) heliocentric distance and exhibited a rapidly changing morphology. These changes were attributed to ions dominating the emission of the coma and emitting mainly in the blue part of the optical spectrum. Different authors published observational results showing that C/2016 R2 had a highly unusual composition: no water molecules (or OH radical) could be detected, and the abundances of commonly observed radicals (CN, C<sub>2</sub>, C<sub>3</sub>) were unusually low, with a surprising coma composition dominated by CO, CO<sub>2</sub>, and N<sub>2</sub> molecules. A high CO production rate of about  $10^{29}$  molecules s<sup>-1</sup> was measured ([Biver et al. 2018](#); [Wierzbach & Womack 2018](#)) as well as a high CO<sub>2</sub> production rate (CO<sub>2</sub>/CO = 1.1 from [Opitom et al. 2019](#)), and a high ratio N<sub>2</sub>/CO that varied between  $\sim 0.06$  and 0.09 ([Biver et al. 2018](#); [Cochran & McKay 2018b,a](#); [Opitom et al. 2019](#); [Venkataramani et al. 2020](#)).

The detection of N<sub>2</sub><sup>+</sup> in the very peculiar comet C/2016 R2 highlighted the necessity of robust modeling of the N<sub>2</sub><sup>+</sup> fluorescence spectrum to enable a quantitative analysis of the amount of N<sub>2</sub> in comets. The high quality of the spectra published by [Opitom et al. \(2019\)](#) also provides a good opportunity to test such a model.

The aim of this paper is to present a first-ever model of the N<sub>2</sub><sup>+</sup> fluorescence spectrum and a comparison of the model with observations. Section 2 presents our observational data, Sect. 3 the model, Sect. 4 compares the model with observational data, and we discuss these results in Sect. 5.

## 2. Observational data

The spectra used for this work have been obtained with the Ultraviolet-Visual Echelle Spectrograph (UVES) mounted on the ESO 8.2 m UT2 telescope of the Very Large Telescope (VLT). They correspond to the dichroic 1 (390+580) setting, covering the range 326–454 nm in the blue and 476–684 nm in the red. We only used the blue part here. Three different observing nights were used, corresponding to February 11, 13, and 14, 2018. During each night, one single exposure of 4800 s of integration time was obtained. We used a 0.44'' wide slit, providing a resolving power of  $R \sim 80\,000$ . The slit length was 8'', corresponding to about 14 500 km at the distance of the comet (geocentric distance of 2.4 au). The average heliocentric distance was 2.76 au and the heliocentric velocity was 5.99 km s<sup>-1</sup>.

As explained in [Opitom et al. \(2019\)](#), the data were reduced using the ESO UVES pipeline, combined with custom routines to perform the extraction and cosmic ray removal, and were then corrected for the Doppler shift due to the relative velocity of the comet with respect to the Earth. The spectra were calibrated in absolute flux using either the archived master response curve or the response curve determined from a standard star observed close to the science spectrum (both were used for C/2016 R2 without significant differences). This data processing produced 2D spectra calibrated in wavelength and absolute flux units. Because a close examination of the ESO UVES sky emission spectrum<sup>1</sup> permits verifying that telluric lines are below the noise level in this part of the spectrum, no specific data processing was made to remove these lines.

<sup>1</sup> [https://www.eso.org/observing/dfo/quality/UVES/pipeline/sky\\_spectrum.html](https://www.eso.org/observing/dfo/quality/UVES/pipeline/sky_spectrum.html)

A close examination of the emission lines permits detecting, as explained in [Opitom et al. \(2019\)](#), numerous emission lines attributed to N<sub>2</sub><sup>+</sup>. The modeling presented Sect. 4 shows the exact match between theoretical and observed wavelengths, computed taking the Doppler shift due to the geocentric velocity into account. This Doppler shift corresponds to a geocentric velocity of 19.9 km s<sup>-1</sup>, that is, to a wavelength shift of 0.26 Å, which is well above the full width at half maximum (FWHM) of the instrument response function (0.06 Å). It clearly separates the cometary lines from the unshifted telluric lines. This good agreement confirms that the detection of N<sub>2</sub><sup>+</sup> in comet C/2016 R2 is robust.

## 3. Model

The transition visible in comets corresponds to the first negative group, that is, the  $B^2\Sigma_u^+ \rightarrow X^2\Sigma_g^+$  electronic transition with the (0, 0) bandhead appearing near 3914 Å. Because they are  $\Sigma$  states, they follow Hund’s coupling case b with a quantum number  $N$  associated with the interaction between the molecule rotation and the electronic orbital angular momentum, and  $J$  is the quantum number associated with the total angular momentum. We have  $J = N \pm 1/2$ .

The selection rules for this transition imply that  $\Delta N = N' - N'' = \pm 1$ . Because two different  $J$  values exist for each value of  $N$  ( $F_1$  and  $F_2$  levels), it is possible to have  $\Delta N = \Delta J$  (main lines labeled P<sub>1</sub>, P<sub>2</sub>, R<sub>1</sub>, and R<sub>2</sub>) or  $\Delta N \neq \Delta J$  (satellite lines <sup>P</sup>Q<sub>12</sub> and <sup>R</sup>Q<sub>21</sub>). Figure 1 presents the energy level diagram with the different types of lines involved in this group.

The spontaneous transition probability for a given line is given by the Einstein coefficients  $A_{v'J' \rightarrow v''J''}$  (expressed in s<sup>-1</sup>) such that

$$A_{v'J' \rightarrow v''J''} = \frac{2 - \delta_{0,\Lambda'}}{2 - \delta_{0,\Lambda'+\Lambda''}} \left( \frac{16\pi^3 \nu^3}{3\epsilon_0 h c^3} \right) | \langle v'N' | \mu_{\Lambda'\Lambda''} | v''N'' \rangle_R |^2 \frac{S_{J'J''}}{(2J' + 1)}, \quad (1)$$

where  $h$  is the Planck constant,  $\nu$  is the frequency,  $c$  is the speed of light,  $| \langle v'N' | \mu_{\Lambda'\Lambda''} | v''N'' \rangle_R |^2$  is the transition dipole moment,  $\delta$  is the Kronecker symbol,  $\epsilon_0$  is the permittivity of the vacuum, and  $S_{J'J''}$  is the Hönl-London factor.  $\Lambda'$  and  $\Lambda''$  are the component of the electronic orbital angular momentum along the internuclear axis of the upper and lower electronic states, respectively. Because these states are  $\Sigma$  states, these numbers are equal to 0, and consequently,  $(2 - \delta_{0,\Lambda'}) / (2 - \delta_{0,\Lambda'+\Lambda''}) = 1$ .

The Einstein coefficients  $A_{v'J' \rightarrow v''J''}$  giving the spontaneous transition probability (in s<sup>-1</sup>) were computed with  $\bar{A}$ ,  $a$ , and  $b$  coefficients computed by [Ferchichi et al. \(2022\)](#) and with the Hönl-London factors given in their Table 4 that were taken from [Mulliken \(1931\)](#). The Einstein absorption coefficients  $B_{v''J'' \rightarrow v'J'}$  were computed from the  $A_{v'J' \rightarrow v''J''}$  coefficients,

$$B_{v''J'' \rightarrow v'J'} = \frac{2J' + 1}{2J'' + 1} \frac{1}{8\pi h \sigma^3} A_{v'J' \rightarrow v''J''}, \quad (2)$$

where  $\sigma$  is the wavenumber (expressed in cm<sup>-1</sup>). The probability of absorption is given by  $B_{v''J'' \rightarrow v'J'} \times \rho_\nu$ , where  $\rho_\nu$  is the radiation density at the corresponding wavelength, expressed in erg cm<sup>-3</sup> Hz<sup>-1</sup>. We used the high-resolution solar spectrum published by [Kurucz et al. \(1984\)](#) to compute the solar radiation density.

The energy levels were computed with the parameters published by [Zhang et al. \(2015\)](#) for the  $X^2\Sigma_g^+$  state and those by

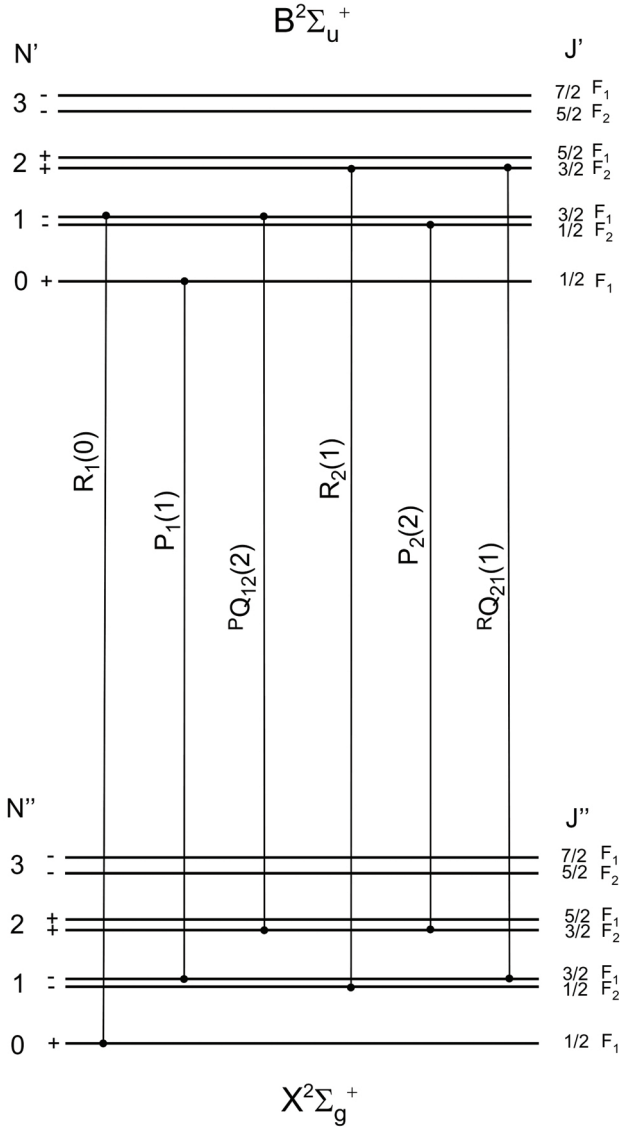


**Fig. 1.** Energy level diagram showing the  $N_2^+$  first negative group  $B^2\Sigma_u^+ \rightarrow X^2\Sigma_g^+$  and the different types of lines allowed by the selection rules. The number in brackets corresponds to the  $N''$  value ( $N$  value in the  $X^2\Sigma_g^+$  state).

Gottscho et al. (1979) for the  $B^2\Sigma_u^+$  state. They were recomputed more accurately for most of the  $v = 0$  and 1 levels (both for the  $X^2\Sigma_g^+$  and  $B^2\Sigma_u^+$  state) using the wavenumbers of the (0, 0), (0, 1), and (1, 1) bands measured by Dick et al. (1978).

Because  $N_2^+$  has no permanent dipole moment, the pure rotational and vibrational transitions are forbidden (or have a very low probability, through quadrupolar transitions; this is not taken into account in our model). For this reason, it takes a long time for this species to reach its fluorescence equilibrium because it needs a few dozen absorption or emission cycles between the  $X^2\Sigma_g^+$  and  $B^2\Sigma_u^+$  states to reach this equilibrium. At the heliocentric distances of C/2016 R2, this corresponds to a few tens of thousands of seconds, or a path of a few tens of thousands of kilometers for the  $N_2^+$  ions inside the coma.

Instead of computing the fluorescence equilibrium, we therefore decided to use a Monte Carlo method similar to the method presented in Rousselot et al. (1994). In this type of method, an initial relative population has to be defined, as well as the time

for which we wish to compute the relative population. A large number of molecules are considered ( $10^5$ ), each of them following a random series of absorption or emission mechanisms based on the computed transition probabilities.

The initial population distribution is in the  $v = 0$  vibrational level of the ground electronic state and follows a Boltzmann distribution such that

$$x_i = \frac{g_i}{Q} e^{-\frac{E_i}{kT}}, \quad (3)$$

with  $T$  the Boltzmann temperature,  $E_i$  the energy value for the level  $i$ ,  $g$  the statistical weight of the considered level, and  $Q$  the partition function, given by

$$Q = \sum_i g_i e^{-\frac{E_i}{kT}}. \quad (4)$$

The statistical weight  $g_i$  is the product of the statistical weight related to the nuclear spin  $g_{ns}$  and  $(2J + 1)$ :  $g_i = g_{ns}(2J + 1)$ .

The statistical weight  $g_{ns}$  can be computed by considering the nuclear spin, and it depends on the considered isotopolog and  $N$  value. For  $^{14}N_2$  we have  $g_{ns} = 6$  for even  $N$  values and  $g_{ns} = 3$  for odd  $N$  values for the  $X^2\Sigma_g^+$  levels. For  $B^2\Sigma_u^+$ , it is the opposite ( $g_{ns} = 3$  for even  $N$  values and  $g_{ns} = 6$  for odd  $N$  values).

We decided to use a Boltzmann temperature close to the kinetic temperature of the gas in the inner coma, that is a few dozen K. We used a value of 80 K, but this parameter has little influence on the final result (the range  $\sim 30$  to  $\sim 200$  K provides similar results for evolution times in the order of a few thousand seconds).

Our Monte Carlo modeling starts with a Boltzmann distribution for the lower states ( $X^2\Sigma_g^+$ ) and provides the relative populations of the levels belonging to this state. From these relative populations, it is easy to compute the relative populations of the upper levels by writing

$$\sum_{j=1}^{N_X} B_{ji} \rho_v = \sum_{j=1}^{N_X} A_{ij} x_i, \quad (5)$$

with  $N_X$  being the number of considered levels in the ground electronic state  $X^2\Sigma_g^+$ , and  $i$  and  $j$  corresponding to the  $i$ th and  $j$ th levels. From this equation, it is possible to compute the relative populations  $x_i$  of the levels belonging to the upper electronic state,

$$x_i = \frac{\sum_{j=1}^{N_X} B_{ji} \rho_v}{\sum_{j=1}^{N_X} A_{ij}}. \quad (6)$$

The luminosity per molecule of a given emission line, also called fluorescence efficiency or  $g$  factor, is given by

$$I = x_i A_{ij}, \quad (7)$$

with  $x_i$  being the relative population of the upper level  $i$  and  $A_{ij}$  the Einstein coefficient corresponding to the transition from the level  $i$  to the level  $j$ . We considered the first three vibrational levels ( $v = 0, 1, 2$ ) for  $X^2\Sigma_g^+$  and  $B^2\Sigma_u^+$ , each of them with all the levels from  $N = 0$  to 40.

Because our observational spectra are in units of  $\text{erg s}^{-1} \text{cm}^{-2} \text{\AA}^{-1}$ , the intensities above were multiplied by  $h\nu$  to obtain units of energy. The observed intensity is then the product of this luminosity per molecule by the number of molecules along the line of sight.

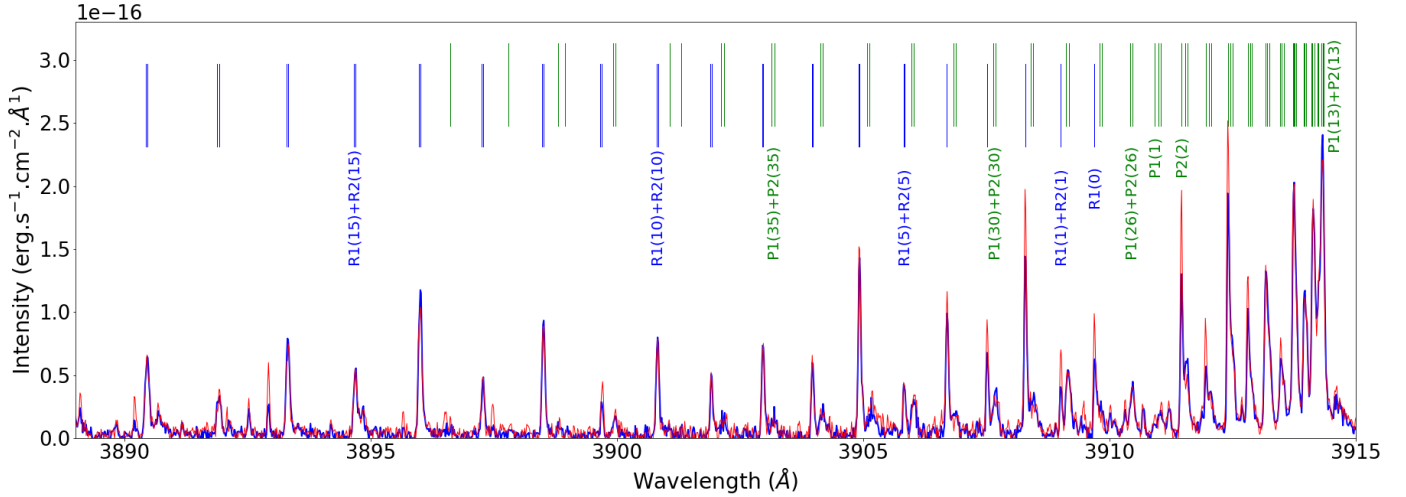


**Fig. 2.** Comparison in red of the observed average spectrum of C/2016 R2 extracted on the nucleus (corresponding to about 250 km on either side of the nucleus) and in blue at the extremity of the slit (cometocentric distance  $\sim 6000$  km). The  $R$  branch of the  $(0, 0)$  band starts at  $3909.7 \text{ \AA}$  and is degraded to the blue side (i.e., lines appear at shorter wavelengths for increasing values of quantum number  $N$ ), and the  $P$  branch starts at  $3910.9 \text{ \AA}$  and returns at the bandhead at  $3914.3 \text{ \AA}$  to shorter wavelengths. Some lines are identified by their type and  $N''$  value (see Fig. 1 for the details), all of them belong to the  $(0, 0)$  band. The two spectra are different.

#### 4. Comparison with observational data

In order to improve the signal-to-noise ratio of the  $N_2^+$  emission lines as much as possible and to confirm the evolution of the emission spectrum with cometocentric distance, we computed average spectra for the three different observing nights and at different cometocentric distances. From the 2D spectra, which have a spatial extent of 30 lines (each of them corresponds to 0.25 arcsec on the slit with different cometocentric distances), we computed an averaged spectrum representative of the region near the nucleus (five rows, centered on the nucleus, in the middle of the slit) and another averaged spectrum representative of the maximum cometocentric distances ( $2 \times 4$  rows at the two extremities of the slit). The solar continuum was subtracted from each spectrum by adjusting a solar spectrum convolved with a similar instrument response function and coming from Kurucz et al. (1984). The artifacts were suppressed before we computed the average spectrum for the three different observing nights.

Figure 2 presents the spectral region near the  $(0, 0)$  bandhead for the spectra obtained on the nucleus and at the end of the slit (corresponding to a varying cometocentric distance of 2.75 and 3.75 arcsec, i.e., between 4800 and 6600 km at that geocentric distance). Some significant differences are clearly seen between these two spectra, confirming that  $N_2^+$  is far from equilibrium in the slit. The relative intensity of lines with low rotational quantum number  $N$  is higher near the nucleus than the intensity of emissions corresponding to regions farther out in the coma. This is typical of relative populations increasing with time, as we could expect from successive absorption or emission cycles with typical lifetimes of about 1000 s each.

From these spectra, we tried realistic parameters to fit the spectrum corresponding to the highest cometocentric distance, that is, to the spectra closer to fluorescence equilibrium that are less dependent on the initial relative population distribution. Because 6000 km corresponds to a projected distance (i.e., to a minimum physical distance to the nucleus), we used an evolution time of 10 000 s (i.e., a rough average estimated from the physical distances to the nucleus; these distances vary along the line of sight from about 6000 km up to infinity with a decreasing

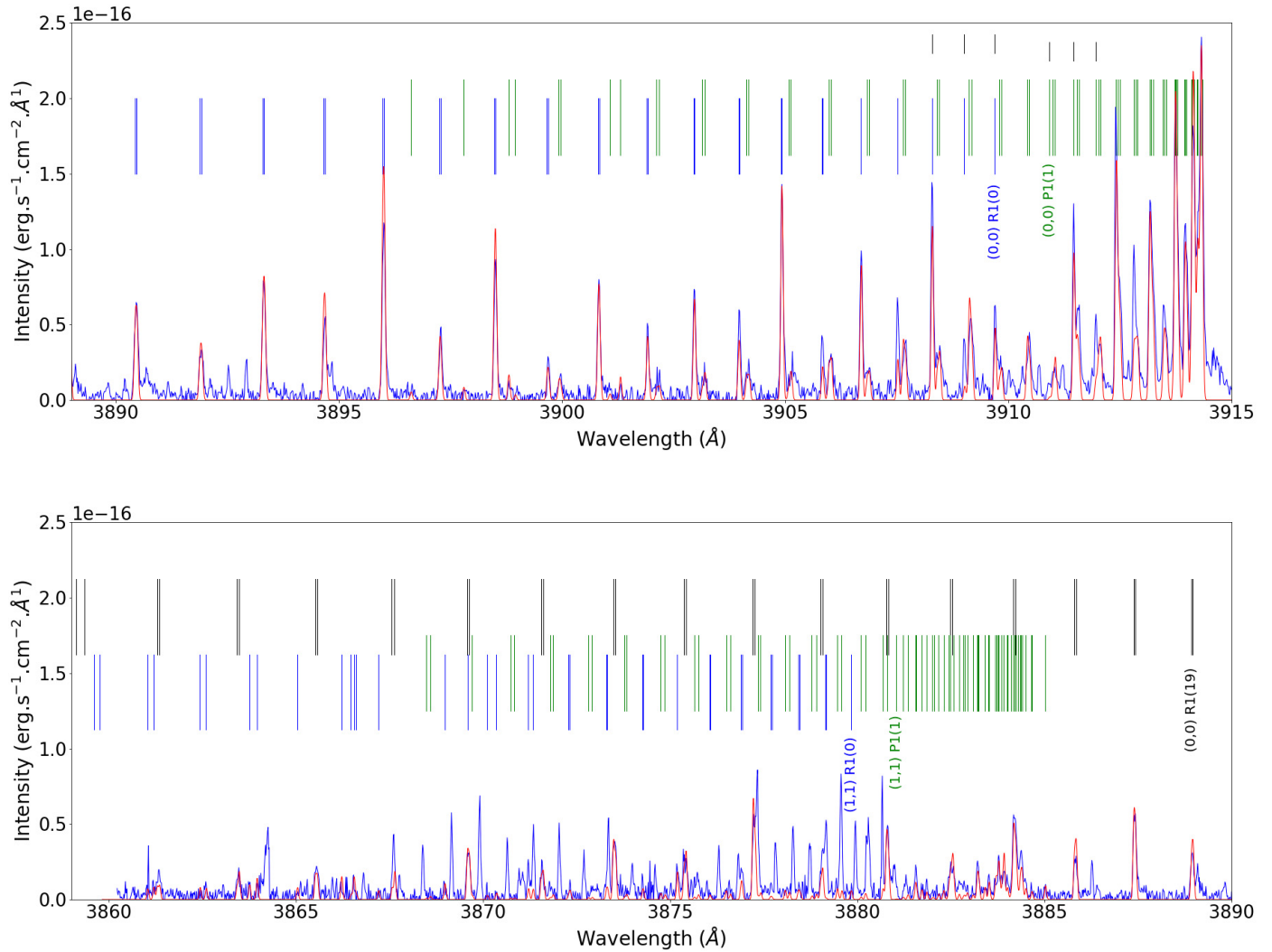
density and an expansion velocity of about  $1 \text{ km s}^{-1}$ ), with an initial Boltzmann distribution corresponding to a temperature of 80 K. This temperature is approximately the kinetic temperature in the inner coma.

The resulting spectrum superimposed on the observations is shown in Fig. 3. Figure 4 shows the emission of the  $(0, 0)$  and  $(1, 1)$  band, respectively, at the same intensity scale. This figure shows that the brightest band is the  $(0, 0)$  and that many emission lines belonging to this band are mixed with those of the  $(1, 1)$  band.

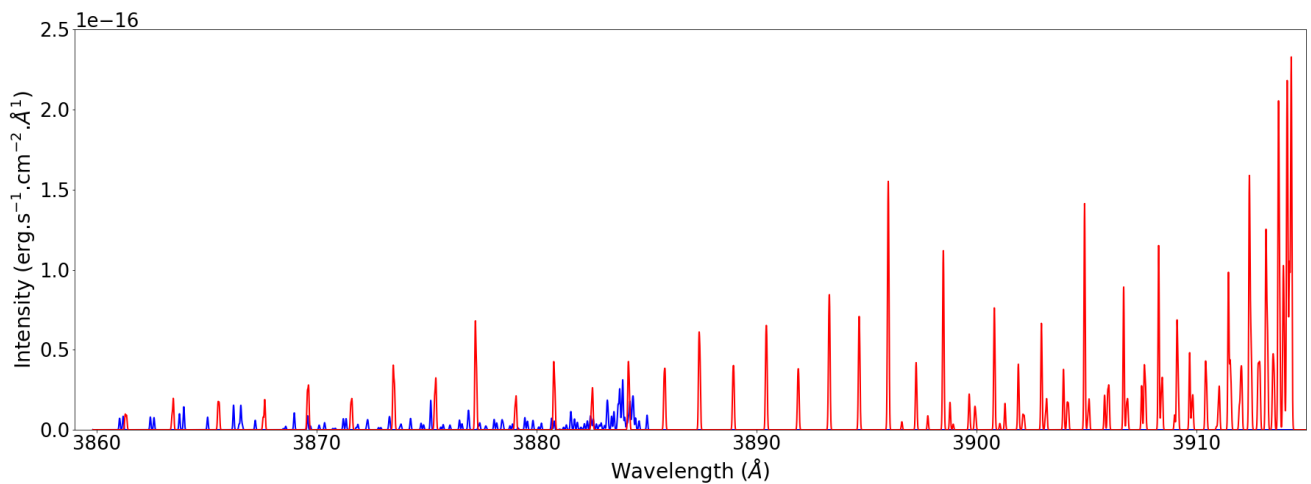
Figure 3 shows that our model is able to reproduce the observed intensities with very good accuracy. It is useful to compute fluorescence efficiencies in order to perform quantitative measurements of the number of  $N_2^+$  molecules along the line of sight. Because the emission lines belonging to the  $(0, 0)$  band and the  $(1, 1)$  band are mixed, as are the CN emission lines, we decided to compute the fluorescence efficiency not only for the  $(0, 0)$  and  $(1, 1)$  bands, but also for the lines of the  $(0, 0)$  band that appear in the spectral region that is not covered by  $(1, 1)$  or CN emission lines. It is also worth highlighting that the emission lines of the  $(0, 0)$  band are still present at wavelengths shorter than the CN emission lines. In some cases, this makes measuring the entire  $(0, 0)$  band intensity difficult.

Table 1 provides the resulting values computed for C/2016 R2 at the time of our observations. Because these factors are usually computed at the reference heliocentric distance of 1 au, this table also provides them for a heliocentric velocity of  $0 \text{ km s}^{-1}$  for all the bands taken into account in our model.

Another interesting result is the importance of the Swings effect, which is related to the influence of the heliocentric velocity on the fluorescence efficiency. The absorption lines in the solar spectrum change significantly, which affects the solar flux that is available for a given transition and, consequently, the relative line intensities. Because a relatively large number of emission lines is involved in this spectrum, this effect is not as strong as for some other radicals (e.g., OH), but it can create a relative variation that reaches about 10%. Table 2 provides the fluorescence efficiencies as a function of heliocentric velocity for the  $(0, 0)$  and  $(1, 1)$  bands. These values are not very sensitive



**Fig. 3.** Comparison of the observed spectra of C/2016 R2 obtained at the edges of the slit (nucleocentric distance  $\sim 6000$  km, averaged at four different lines at the two extremities of the slit) with the model. The upper and lower parts corresponds to two different wavelengths intervals. Some CN emission lines, not reproduced by the model, appear in the region around  $3880$  Å. The observational data are plotted in blue, and the modeling is shown in red. For more clarity, the wavelengths of the observed lines are given by vertical bars above the spectra. The  $R$  branch is degraded to the blue side, and the  $P$  branch is first degraded to the red side and returns to the bluer wavelengths after the bandhead. The first three  $^PQ_{12}$  and  $^RQ_{21}$  satellite lines are also plotted above (vertical black bars at about  $3910$  Å). Their intensity is negligible compared to the  $P$  or  $R$  lines for higher values of  $N$ .



**Fig. 4.** Theoretical spectrum showing separately the (0, 0) and the (1, 1) emission band of  $N_2^+$  (red and blue, respectively).

**Table 1.** Fluorescence efficiency ( $g$  factor) in photons  $s^{-1}$  ion $^{-1}$  computed for comet C/2016 R2 at the time of observations and for any comet at 1 au and a heliocentric velocity of 0.0 km  $s^{-1}$ .

| Band ( $v', v''$ )    | $g$                   | $g$ (at 1 au)         |
|-----------------------|-----------------------|-----------------------|
| (0, 0)                | $6.26 \times 10^{-3}$ | $4.90 \times 10^{-2}$ |
| (0, 0)[3885.5–3915 Å] | $5.41 \times 10^{-3}$ |                       |
| (0, 1)                | $2.05 \times 10^{-3}$ | $1.59 \times 10^{-2}$ |
| (0, 2)                | $4.22 \times 10^{-4}$ | $3.31 \times 10^{-3}$ |
| (1, 0)                | $1.43 \times 10^{-3}$ | $1.08 \times 10^{-2}$ |
| (1, 1)                | $9.65 \times 10^{-4}$ | $7.24 \times 10^{-3}$ |
| (1, 2)                | $1.02 \times 10^{-3}$ | $7.67 \times 10^{-3}$ |
| (2, 0)                | $1.67 \times 10^{-4}$ | $1.24 \times 10^{-3}$ |
| (2, 1)                | $1.39 \times 10^{-3}$ | $1.04 \times 10^{-2}$ |
| (2, 2)                | $1.58 \times 10^{-4}$ | $1.18 \times 10^{-3}$ |

**Notes.** For C/2016 R2, the heliocentric distance is 2.76 au and the heliocentric velocity is  $-5.99$  km  $s^{-1}$ . The  $g$  factor restricted to the [3885.5–3915 Å] wavelength range is not given for 1 au because it cannot be simply compared to the factor computed for the heliocentric distance of C/2016 R2. The relative intensities between the different lines are different.

to the cometocentric distance or to the time elapsed since the initial population distribution because so many emission lines are involved in these bands.

The results given in these tables are not very sensitive to the modeling parameters (i.e., initial kinetic temperature or elapsed time, with reasonable limits of at least a few thousand seconds). When these values were computed for different heliocentric distances, they followed the  $r_h^{-2}$  dependence very well. The number of molecules taken into account in our Monte Carlo simulation ( $10^5$ ) provided an uncertainty of about one digit in these tables.

The only  $g$  factors published for  $N_2^+$  so far were computed by Lutz et al. (1993). Their computation corresponds to an approximation for the whole band. Their value for the (0, 0) band is slightly higher than our computed value (they found  $g(0, 0) = 7 \times 10^{-2}$  photon  $s^{-1}$  ion $^{-1}$  for 1 au). Our method of computation, which takes all the lines into account one by one, and compares them to an observational spectrum, is more accurate. A good test is computing the ratio of the fluorescence efficiencies of the (1, 1) band to the (0, 0) band. From the fluorescence efficiencies published by Lutz et al. (1993), this ratio is  $5.1 \times 10^{-3} / 7.0 \times 10^{-2} = 0.0728$ . In our results, it is close to 0.15 (either based on data for 1 au and 0 km  $s^{-1}$  or based on data computed for C/2016 R2), that is, twice the ratio computed by Lutz et al. (1993). Figure 3 clearly shows that the ratio we computed is very close to the observed spectrum. A ratio twice lower is clearly far from the observed intensity ratio.

## 5. Discussion

We presented the first modeling of the  $N_2^+$  fluorescence emission spectrum in a comet. The main difficulty in computing such a spectrum is related to the lack of pure vibrational and rotational transitions, which means that a long time is required to reach fluorescence equilibrium. The spectra obtained in the near nucleus region, which is the usually observed region in cometary comae to obtain spectra with the best signal-to-noise ratio, cannot be interpreted with the normal methods of computation based on a steady-state solution. With our model, which was developed on the basis of a Monte Carlo method, the important parameter is

**Table 2.** Fluorescence efficiency ( $g$  factor) in photons  $s^{-1}$  ion $^{-1}$  computed at 1 au and different heliocentric velocities  $\dot{r}_h$ .

| $\dot{r}_h$ (km $s^{-1}$ ) | (0, 0)                | (1, 1)                |
|----------------------------|-----------------------|-----------------------|
| -20                        | $4.64 \times 10^{-2}$ | $6.98 \times 10^{-3}$ |
| -18                        | $4.60 \times 10^{-2}$ | $6.66 \times 10^{-3}$ |
| -16                        | $4.76 \times 10^{-2}$ | $6.88 \times 10^{-3}$ |
| -14                        | $4.79 \times 10^{-2}$ | $7.11 \times 10^{-3}$ |
| -12                        | $4.76 \times 10^{-2}$ | $7.24 \times 10^{-3}$ |
| -10                        | $4.64 \times 10^{-2}$ | $7.31 \times 10^{-3}$ |
| -8                         | $4.62 \times 10^{-2}$ | $7.41 \times 10^{-3}$ |
| -6                         | $4.72 \times 10^{-2}$ | $7.60 \times 10^{-3}$ |
| -4                         | $4.77 \times 10^{-2}$ | $7.85 \times 10^{-3}$ |
| -2                         | $4.84 \times 10^{-2}$ | $7.39 \times 10^{-3}$ |
| 0                          | $4.90 \times 10^{-2}$ | $7.24 \times 10^{-3}$ |
| +2                         | $4.95 \times 10^{-2}$ | $7.27 \times 10^{-3}$ |
| +4                         | $4.97 \times 10^{-2}$ | $7.40 \times 10^{-3}$ |
| +6                         | $4.93 \times 10^{-2}$ | $7.57 \times 10^{-3}$ |
| +8                         | $4.88 \times 10^{-2}$ | $7.67 \times 10^{-3}$ |
| +10                        | $4.79 \times 10^{-2}$ | $7.65 \times 10^{-3}$ |
| +12                        | $4.73 \times 10^{-2}$ | $7.59 \times 10^{-3}$ |
| +14                        | $4.68 \times 10^{-2}$ | $7.53 \times 10^{-3}$ |
| +16                        | $4.63 \times 10^{-2}$ | $7.56 \times 10^{-3}$ |
| +18                        | $4.62 \times 10^{-2}$ | $7.67 \times 10^{-3}$ |
| +20                        | $4.62 \times 10^{-2}$ | $7.77 \times 10^{-3}$ |

the time that has elapsed from an initial Boltzmann distribution of the relative populations.

Most of the species in cometary comae (with emission lines in the optical region) rapidly reach their fluorescence equilibrium because they are heteronuclear molecules and pure rotational and vibrational electric dipole transitions are allowed. The main exception is the  $C_2$  radical, which shows hundreds of emission lines in the Swan bands because pure rotational and vibrational electric dipole transitions are forbidden and only intercombination transitions (with a low probability) permit this radical to deexcite to lower rotational and vibrational levels (Rousselot et al. 2000).

The  $N_2^+$  ions located along the line of sight correspond to different elapsed times since their creation, mainly by photoionization (see Raghuram et al. 2021 for more details about an estimate of the different processes leading to the formation of  $N_2^+$  ions in the inner coma of comet C/2016 R2). Modeling the resulting spectrum that is created by ions with different emission spectra is therefore difficult. This work shows that we can obtain an acceptable result for the spectra obtained at the end of the slit, but this cometocentric distance remains relatively small compared to the distance needed to reach a complete fluorescence equilibrium.

A good test of our model and of how the different parameters might be adjusted would be to obtain spectra at shorter heliocentric distances and larger cometocentric distances. We would expect to be closer to the fluorescence equilibrium because the number of absorption or emission cycles are more important for a given time at shorter heliocentric distances (the solar radiation density is higher).

The revised values for the fluorescence efficiencies computed in this work imply some revisions for the relative abundances of  $N_2^+$  compared to  $CO^+$ , for which they have been published and based on the calculations of Lutz et al. (1993).

Opitom et al. (2019) reported a N<sub>2</sub><sup>+</sup>/CO<sup>+</sup> ratio of  $0.06 \pm 0.01$ , which agrees well with Cochran & McKay (2018b,a) and Raghuram et al. (2021). Because this ratio is proportional to the ratio of the CO<sup>+</sup> fluorescence efficiency to the efficiency of N<sub>2</sub><sup>+</sup>, the final N<sub>2</sub><sup>+</sup>/CO<sup>+</sup> ratio is expected to change from 6% to 8.8% if  $g_{\text{N}_2^+}$  changes from  $7 \times 10^{-2}$  to  $4.77 \times 10^{-2}$  photon s<sup>-1</sup> ion<sup>-1</sup> (i.e., the value computed for the time of observation scaled to 1 au).

## 6. Conclusion

We were able to model for the first time the emission spectrum of N<sub>2</sub><sup>+</sup> ions in a cometary coma based on high-quality and high-resolution spectra observed at different cometocentric distances. The data available from the literature enabled a modeling based on a Monte Carlo simulation, which provided a good fit of the observed spectrum. The main free parameter was the elapsed time since the initial relative population. Other observations of N<sub>2</sub><sup>+</sup> spectrum are welcome so that the accuracy of this model can be tested. The different fluorescence efficiencies computed with our model are given in Tables 1 and 2 and allow a more detailed quantitative study of this species, which is rare in comets.

Comets that are rich in hypervolatiles species such as N<sub>2</sub><sup>+</sup> and CO<sup>+</sup> are interesting for a better understanding of the origin of comets. These species are often observed at large heliocentric distances, and they place some constraints on the physical properties at their place of formation and the differences of initial chemical composition in the protosolar nebula that explain the currently observed difference of chemical compositions in comets. In this context, the modeling of the N<sub>2</sub><sup>+</sup> fluorescence spectrum and the fluorescence efficiencies computed in this work can help to interpret future observations better.

Some improvements of our model will be made, for instance, for computing the emission spectrum of <sup>14</sup>N<sup>15</sup>N<sup>+</sup>. Even if the detection of such an isotopolog is challenging, future observing facilities currently under construction (e.g., the Extremely Large Telescope built by the European Southern Observatory) open the possibilities for such a detection in other comets that are rich in N<sub>2</sub>.

*Acknowledgements.* Based on observations made with ESO Telescopes at the La Silla Paranal Observatory under program 2100.C-5035(A). This work was

supported by Bourgogne Franche-Comté region (DIAZOTE project). E.J., D.H. and J.M. are senior research associate, research director, and honorary research director at the F.R.S.-FNRS, respectively.

## References

- Biver, N., Bockelée-Morvan, D., Paubert, G., et al. 2018, *A&A*, 619, A127  
 Cochran, A. L., & McKay, A. J. 2018a, *ApJ*, 856, L20  
 Cochran, A. L., & McKay, A. J. 2018b, *ApJ*, 854, L10  
 Cruikshank, D. P., Roush, T. L., Owen, T. C., et al. 1993, *Science*, 261, 742  
 de La Baume Pluvinel, A., & Baldet, F. 1911, *ApJ*, 34, 89  
 Dick, K. A., Benesch, W., Crosswhite, H. M., et al. 1978, *J. Mol. Spectr.*, 69, 95  
 Ferchichi, O., Derbel, N., Alijah, A., & Rousselot, P. 2022, *A&A*, 661, A132  
 Gottscho, R. A., Field, R. W., Dick, K. A., & Benesch, W. 1979, *J. Mol. Spectr.*, 74, 435  
 Greenstein, J. L. 1962, *ApJ*, 136, 688  
 Iro, N., Gautier, D., Hersant, F., Bockelée-Morvan, D., & Lunine, J. I. 2003, *Icarus*, 161, 511  
 Ivanova, O. V., Luk'yanyk, I. V., Kiselev, N. N., et al. 2016, *Planet. Space Sci.*, 121, 10  
 Ivanova, O. V., Picazzio, E., Luk'yanyk, I. V., Cavichia, O., & Andrievsky, S. M. 2018, *PASS*, 157, 34  
 Korsun, P. P., Ivanova, O. V., & Afanasiev, V. L. 2008, *Icarus*, 198, 465  
 Korsun, P. P., Rousselot, P., Kulyk, I. V., Afanasiev, V. L., & Ivanova, O. V. 2014, *Icarus*, 232, 88  
 Kurucz, R. L., Furenlid, I., Brault, J., & Testerman, L. 1984, *Solar flux atlas from 296 to 1300 nm* (New Mexico: National Solar Observatory)  
 Levison, H. F. 1996, *Completing the Inventory of the Solar System*, *ASP Conf. Ser.*, 107, eds. T. Rettig, & J. M. Hahn, 173  
 Lutz, B. L., Womack, M., & Wagner, R. M. 1993, *ApJ*, 407, 402  
 Merlin, F., Lellouch, E., Quirico, E., & Schmitt, B. 2018, *Icarus*, 314, 274  
 Mousis, O., Guilbert-Lepoutre, A., Lunine, J. I., et al. 2012, *ApJ*, 757, 146  
 Mousis, O., Aguichine, A., Bouquet, A., et al. 2021, *PSJ*, 2, 72  
 Mulliken, R. S. 1931, *Rev. Mod. Phys.*, 3, 89  
 Opitom, C., Hutsemékers, D., Jehin, E., et al. 2019, *A&A*, 624, A64  
 Owen, T. C., Roush, T. L., Cruikshank, D. P., et al. 1993, *Science*, 261, 745  
 Quirico, E., Douté, S., Schmitt, B., et al. 1999, *Icarus*, 139, 159  
 Raghuram, S., Bhardwaj, A., Hutsemékers, D., et al. 2021, *MNRAS*, 501, 4035  
 Rousselot, P., Clairemidi, J., & Moreels, G. 1994, *A&A*, 286, 645  
 Rousselot, P., Hill, S. M., Burger, M. H., et al. 2000, *Icarus*, 146, 263  
 Rubin, M., Altwegg, K., Balsiger, H., et al. 2015, *Science*, 348, 232  
 Rubin, M., Engrand, C., Snodgrass, C., et al. 2020, *Space Sci. Rev.*, 216, 102  
 Venkataramani, K., Ganesh, S., & Baliyan, K. S. 2020, *MNRAS*, 495, 3559  
 Weryk, R., & Wainscoat, R. 2016, *Central Bureau Electronic Telegrams*, 4318  
 Wierzbos, K., & Womack, M. 2018, *AJ*, 156, 34  
 Wyckoff, S., & Theobald, J. 1989, *Adv. Space Res.*, 9, 157  
 Zhang, Y.-p., Deng, L.-h., Zhang, J., & Chen, Y.-q. 2015, *Chinese J. Chem. Phys.*, 28, 134